Defect and Diffusion Forum Vols. 237-240 (2005) pp. 603-608
online at http://www.scientific.net

The temperature influence on the faceting of Σ3 grain boundaries in aluminium

Olga Kogtenkova[1,a], Boris Straumal[1,b], Svetlana Protasova[1,c], Pawel Zięba[2,d]

[1]Institute of Solid State Physics, Russian Academy of Sciences, Chernogolovka, Moscow District, 142432 Russia
[2]Institute of Metallurgy and Materials Science, Polish Academy of Sciences, Reymonta St. 25, 30-059 Cracow, Poland
[a]koololga@issp.ac.ru, [b]straumal@issp.ac.ru, [c]sveta@issp.ac.ru, [c]nmzieba@imim-pan.krakow.pl

Keywords: grain boundaries, faceting, roughening, Al, sigma-3, phase diagrams

Abstract. Grain boundary faceting can strongly influence the diffusion permeability of polycrystals and other diffusion-controlled phenomena like grain growth, grain sliding, etc. Faceting is a well known phenomenon for the grain boundary behaviour. Faceting can be considered as a phase transition when the grain boundary dissociates onto flat segments whose energy is less than that for the original grain boundary. For the investigation of grain boundary faceting a cylindrical Al bicrystal of 99.999% wt. purity was grown by the Bridgman technique. One grain in this bicrystal is semi-surrounded by another one. The bicrystal contains a coincidence tilt grain boundary Σ3 <110>. Bicrystalline samples were coated with a layer of Sn–Al mixture and annealed at different temperatures: 723 and 873 K. Contact angles at the junction of grain boundary and two solid/liquid interfaces were measured. Ratio of grain boundary energy and solid/liquid interface energy had been calculated. Wulff-Herring plots and grain boundary phase diagrams were constructed. Three crystallographic different facets were observed. Two of them remain stable at 723 K, the third one becomes metastable.

Introduction

Faceting is a well documented phenomenon known both for surfaces and interfaces, particularly, grain boundaries [1–4]. Faceting can be considered as a phase transition when the original surface or grain boundary dissociates into flat segments whose energy is less than that of the original surface or grain boundary. Grain boundary faceting proceeds only close to so-called coincidence misorientations. In this case the lattices of both grains form the coincidence site lattice (CSL) characterized by the parameter Σ (reverse density of coincidence sites). In most cases the grain boundary facets lie in the CSL planes with high density of coincidence sites. It has been shown [5] that grain boundaries possess special structure and properties in limited areas of temperature T and misorientation θ close to a coincidence misorientation, θ_Σ. In other words, by increasing $\Delta\theta = |\theta - \theta_\Sigma|$ and T the phase transition "special grain boundary – general grain boundary" proceeds and the grain boundary losses its special structure and properties [6]. This is due to the fact that for the CSLs with low Σ the depth of the energetic profile for the close packed CSL planes is larger than that of high-Σ CSLs. Therefore, due to the temperature disordering the energetically favourable grain boundary positions disappear at lower T for grain boundaries with higher Σ [7]. We can expect that at high temperature only the facets with highest density of coincidence sites would appear.

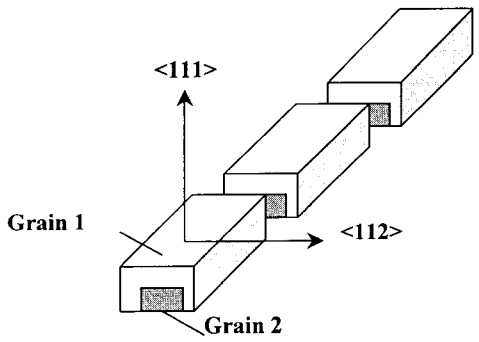

Fig. 1. Schematic view of the bicrystalline samples.

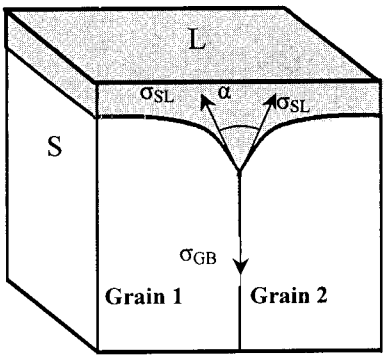

Fig. 2. Scheme of the equilibrium contact between the grain boundary in the solid phase **S** and the liquid phase **L** (incomplete wetting).

Experimental

For the investigation of grain boundary faceting an Al (99.999 wt.% purity) bicrystal with a semi-island grain was grown using the modified Bridgman technique. Grain *2* in this bicrystal is semi-surrounded by grain *1* forming the Σ3 <110> tilt grain boundary (Fig. 1). 5 mm thick platelets were cut from the grown bicrystal perpendicularly to the growth axis. The bicrystalline samples were coated with a layer of Sn–Al mixture and annealed in Ar gas atmosphere at pressure of 2×10^{-4} Pa and temperatures 723 and 873 K during 2 hours. Then the samples were mechanically ground, polished and etched in 50% HNO_3+47% HCl+3%HF solution. To determine the ratio between grain boundary energy, σ_{GB}, and solid/liquid interface energy, σ_{SL}, the contact angle α is measured (Fig. 2). The contact angle α and geometry of facets were analyzed and recorded in bright and dark field in light microscope (Figs. 3 and 4).

The ratio between grain boundary energy σ_{GB} and solid/liquid interface energy σ_{SL} was calculated using the values of measured contact angle α:

$$\sigma_{GB} = 2\sigma_{SL}\cos(\alpha/2)$$

Micrograph of the Σ3 grain boundary is shown in Fig. 4.

The electron back-scattering diffraction (EBSD) method was used to determine the individual grain orientations in the Al bicrystals and the grain boundary shape in the as-grown bicrystals. The orientation spread in both grains of bicrystal was below 0.5°. The EBSD method permits observation of the sample microstructure and determination of the individual grain orientation in the same experiment. The EBSD-patterns were measured using a Hitachi S-4200 scanning electron microscope. The spatial resolution in the EBSD regime reaches 50 nm. Due to the large sample area, the steps between analysis points were 10 μm. We determined the individual grain orientation using the EBSD patterns and integrated software package for semi-automated fit procedure. In the samples under the investigation the misorientation deviation from coincidence tilt grain boundary Σ3 <110> was less then 1° along the grain boundary. It was significant that there were no triple junctions in the corners of the semi-surrounded grain, where the facets intersect.

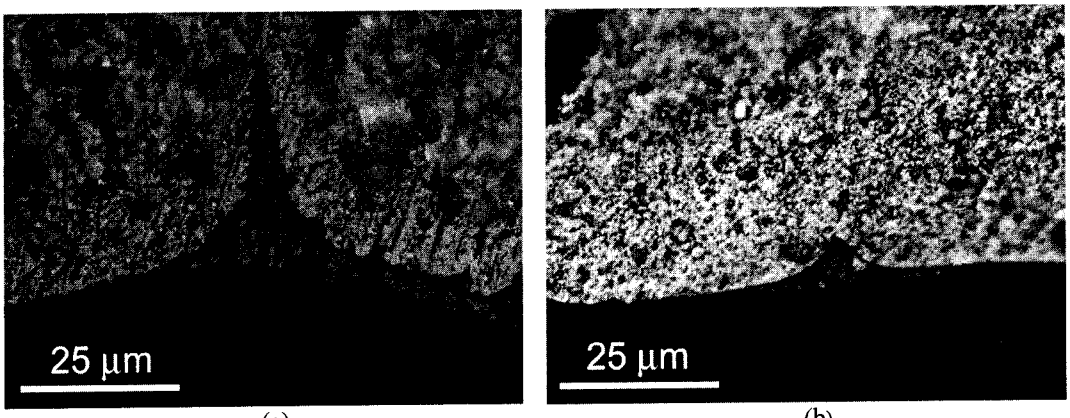

(a) (b)

Fig. 3. The contact angle α of grain boundary Σ3 on different facets: (a) $(100)_{\Sigma 3CSL}$ facet; (b) 9*R* facet at 873 K.

Results and discussion

In Σ3 grain boundaries three different facets were observed, namely symmetric Σ3 twin boundaries $\{111\}_1/\{111\}_2$ [or $(100)_{\Sigma 3CSL}$] facets, the facet with an angle of 82° with the symmetric twin boundary, and the $\{100\}_1/\{122\}_2$ [or $(110)_{\Sigma 3CSL}$] facets. The $(110)_{\Sigma 3CSL}$ facet has an angle of 56° with $(100)_{\Sigma 3CSL}$ facet. The section of Σ3 CSL perpendicular to the <110> axis is shown in the Fig. 5. The most close packed CSL planes are shown together with the respective planes for the lattices *1* and *2* forming CSL.

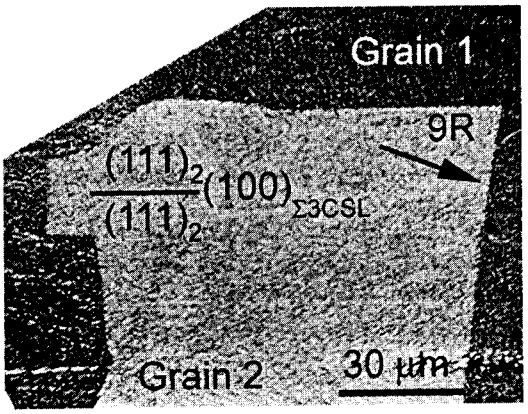

Fig. 4. Light micrograph showing the shape of Σ3 grain boundary.

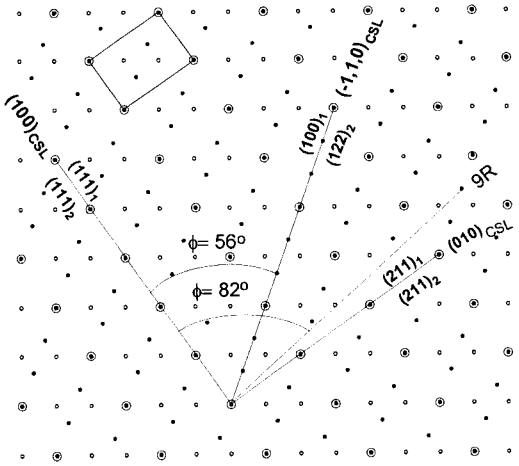

Fig. 5. Section of Σ3 CSL perpendicular to the {110} tilt axis with CSL unit cell and positions of $(100)_{\Sigma 3CSL}$ and $(010)_{\Sigma 3CSL}$ facets.

In Fig. 6 the Wulff-Herring plot is shown for Σ3 grain boundaries at different temperatures. The Wulff-Herring plot was constructed using the σ_{GB}/σ_{SL} ratios measured by light microscopy.

The energy of symmetric Σ3 twins $\{111\}_1/\{111\}_2$ [or $(100)_{\Sigma3CSL}$] facet is very low. These facets are very stable and observed at different temperatures (Fig. 6). The next closely packed CSL plane is $\{211\}_1/\{211\}_2$ [or $(010)_{\Sigma3CSL}$] or so-called asymmetric twin. The angle between $(100)_{\Sigma3CSL}$ and $(010)_{\Sigma3CSL}$ facets is 90°. The presence of such facets are well documented for Al, Au, $AuCu_3$, and Ge [8–11]. The typical rectangular twin plates with $(100)_{\Sigma3CSL}$ and $(010)_{\Sigma3CSL}$ facets can be seen, for example in Au thin films [9]. However, the twin plates in Cu and Ag are not rectangular. The end facet forms an angle of 82° with the $\{111\}_1/\{111\}_2$ or $(100)_{\Sigma3CSL}$ sides [12, 13]. TEM studies revealed that this 82° facet has so-called 9*R* structure forming a plate of bcc grain boundary phase in the fcc matrix [14–17]. Such $(100)_{\Sigma3CSL}$ and 82° 9*R* facets on the Σ3 twin plate are clearly seen also in our samples in Fig. 4. Moreover, analysis of the available data shows that the 82° 9*R* facet appears in Cu only at high temperatures. At low temperatures the "normal" 90° $(010)_{\Sigma3CSL}$ facets are present in Cu [17]. The 82° 9*R* facet appears instead of the 90° $(010)_{\Sigma3CSL}$ facet at high temperature. In our samples the 82° 9*R* facet is present at high temperature, but the 90° $(010)_{\Sigma3CSL}$ facet was not observed at low temperature. It is significant that grain boundary shape was stable at very high temperature (close to the melting point) during long-term annealing of the samples. Therefore, we suppose that this is an equilibrium shape for the investigated samples.

The facet 56° with the $\{100\}_1/\{122\}_2$ [or $(110)_{\Sigma3CSL}$] was also observed in the studied grain boundary. This facet is present within a wider range of temperature and annealing time in contrast to Cu. However, the angle interval ψ, where this facet is stable becomes narrower with the temperature increasing (Fig. 7). It can be supposed that near the melting point the facet $\{100\}_1/\{122\}_2$ [or $(110)_{\Sigma3CSL}$] would disappear.

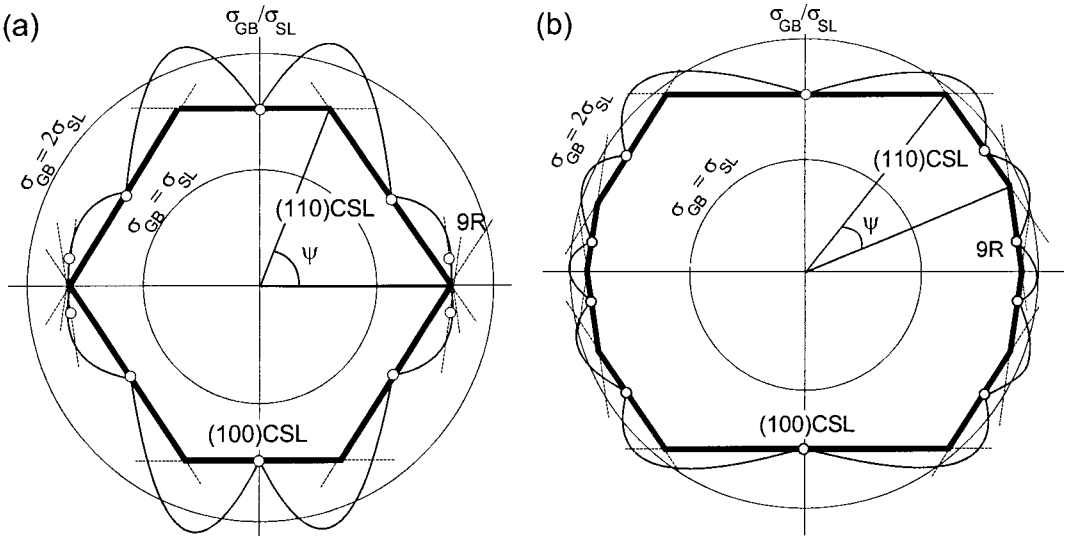

Fig. 6. Wulff-Herring plot for the Σ3 grain boundary at different temperatures: (a) 723 K, (b) 873 K. Thick solid lines denote the equilibrium grain boundary shape.

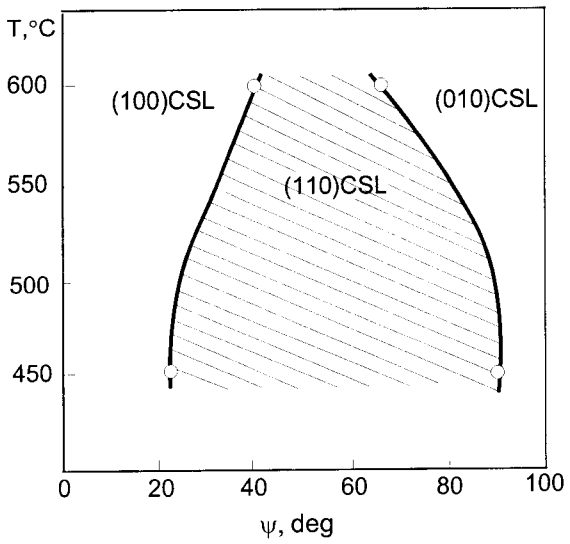

Fig. 7. Schematic view of angle interval ψ of the $\{100\}_1/\{122\}_2$ [or $(110)_{\Sigma 3CSL}$] facet stability.

Conclusions

The Wulf-Herring plots constructed demonstrate, that by decreasing temperature the $(110)_{\Sigma 3CSL}$ facet becomes more and more stable. However, the non-CSL facet 9*R* becomes unstable already at 723 K = 0,77 T_m (T_m is the melting temperature). Therefore, the 9*R* facet also in Al, similar to Cu and Ag, is stable only close to melting temperature. Even close to this temperature all facets form sharp edges at their intersection (similar to Cu [17]). Therefore, no indication of grain boundary roughening occurs. However, such grain boundary roughening is very pronounced in Σ3 grain boundary in Mo, a metal having bcc lattice [18].

Acknowledgements

This work was supported by the Russian Foundation of Basic Research (contracts 03-02-16947 and 03-02-04000), INTAS Programme under contract 99-1216, NATO Linkage grant (PST.CLG.979375), German Federal Ministry for Education and Research (BMBF) under WTZ-Project RUS 04/014, and exchange programme between Russian and Polish Academies of Sciences.

References

[1] S. B. Lee, D.Y. Yoon and M.F. Henry: Acta mater. Vol. 48 (2000), p. 3071.
[2] M. Yoon, S.G.J. Mochrie, M.V. Tate, S.M. Gruner and E.F. Eikenberry: Surf. Sci. Vol. 70 (1998), p. 411.
[3] G.M. Watson, D. Gibbs, S. Song, A.R. Sandy, S.G.J. Mochrie and D.M. Zener: Phys. Rev. B Vol. 52 (1995), p. 12329.
[4] S. Song and S.G.J. Mochrie: Phys. Rev. B Vol. 51 (1995), p. 10068.
[5] B.B. Straumal and L.S. Shvindlerman: Acta metall. Vol 33 (1985), p. 1735.
[6] E.L. Maksimova, L.S. Shvindlerman and B.B. Straumal: Acta metall. Vol. 36 (1998), p. 1573.
[7] A.A. Zisman and V.V. Rybin: Poverkhnost', No. 7, Vol. 87 (1982) in Russian.
[8] J.M. Pénisson, U. Dahmen and M.J. Mills: Phil. Mag. Lett. Vol. 64 (1991), p. 277.

[9] P.J. Goodhew, T.Y. Tan and R.W. Balluffi: Acta metall. Vol. 26 (1978), p. 557.
[10] F.D. Tichelaar and F.W. Schapink: J. Phys. Paris, C5, Vol. 49 (1988), p. 293.
[11] A. Bourret and J.J. Bacmann: Inst. Phys. Conf. Series Vol. 78 (1985), p. 337.
[12] T. Muschik, W. Laub, M.W. Finnis and W. Gust: Z. Metallk. Vol. 84 (1993), p. 596.
[13] A. Barg, E. Rabkin and W. Gust: Acta metall. mater. Vol. 43 (1995), p. 4067.
[14] U. Wolf, F. Ernst, T. Muschik, M.W. Finnis and H.F. Fischmeister: Phil. Mag. A Vol. 66 (1992), p. 991.
[15] F. Ernst, M.W. Finnis, D. Hoffmann, T. Muschik, U. Schönberger and U. Wolf: Phys. Rev. Lett. Vol. 69 (1992), p. 620.
[16] D. Hofmann and M.W. Finnis: Acta metall. mater. Vol. 42 (1994), p. 3555.
[17] B.B. Straumal, S.A. Polyakov, E. Bischoff, W. Gust and E.J. Mittemeijer: Interface Sci. Vol. 9 (2001), p. 287.
[18] B.B. Straumal, V.N. Semenov, O.A. Kogtenkova and T. Watanabe: Phys. Rev. Lett. Vol. 192 (2004), p. 196101.